© 2022. Published by The Company of Biologists Ltd | Development (2022) 149, dev200516. doi:10.1242/dev.200516

RESEARCH ARTICLE

CCDC38 is required for sperm flagellum biogenesis and male fertility in mice

Ruidan Zhang[1,2,3,*], Bingbing Wu[1,2,3,*], Chao Liu[1,2], Zhe Zhang[4,5,6,7], Xiuge Wang[1,3], Liying Wang[1,2], Sai Xiao[1,3], Yinghong Chen[1,3], Huafang Wei[1,2], Hui Jiang[4,5,6,7,‡], Fei Gao[1,3,‡], Li Yuan[8,‡] and Wei Li[1,2,‡]

ABSTRACT

The sperm flagellum is essential for male fertility, and defects in flagellum biogenesis are associated with male infertility. Deficiency of coiled-coil domain-containing (CCDC) 42 (CCDC42) is specifically associated with malformation of mouse sperm flagella. Here, we find that the testis-specific protein CCDC38 interacts with CCDC42, localizing on the manchette and sperm tail during spermiogenesis. Inactivation of CCDC38 in male mice results in a distorted manchette, multiple morphological abnormalities of the flagella of spermatozoa and eventually male sterility. Furthermore, we find that CCDC38 interacts with intraflagellar transport protein 88 (IFT88), as well as outer dense fibrous 2 (ODF2), and the knockout of *Ccdc38* reduces transport of ODF2 to the flagellum. Altogether, our results uncover the essential role of CCDC38 in sperm flagellum biogenesis, and suggest that some mutations of these genes might be associated with male infertility in humans.

KEY WORDS: MMAF, CCDC38, IFT88, ODF2, Flagellum biogenesis

INTRODUCTION

The sperm flagellum is essential for sperm motility (Freitas et al., 2017; Pereira et al., 2017), which is a fundamental requirement for male fertility. The flagellum contains four parts: connecting piece, midpiece, principal piece and end piece. The core of the sperm flagellum is the central axoneme, which consists of a central microtubule pair connected to nine peripheral outer microtubule doublets to form a '9+2' structure (Sironen et al., 2020). The axoneme possesses radial spokes that connect the central and peripheral microtubules and are related to the mechanical movement of the flagellum (Inaba, 2011). Besides the axoneme, the sperm flagellum contains unique structures, the outer dense fibers (ODFs) and the fibrous sheath (FS), that are not present in cilia or unicellular flagella (Fawcett, 1975). The ODFs are the main cytoskeletal elements of sperm flagella, which are required for sperm motility (Inaba, 2011). ODFs contain nine fibers in the midpiece, each of which is associated with a microtubule doublet. In humans, ODFs 3 and 8 in the principal piece are replaced by two longitudinal columns of FS, with diminished fibers 3 and 8 ending at the annulus (Azizi and Ghafouri-Fard, 2017; Kim et al., 1999). There are at least 14 proteins that make up the ODFs, including ODF1 and ODF2 (Lehti and Sironen, 2017). Any defects in the axoneme structure can cause abnormalities in the sperm flagellum by changing the morphology and causing severe sperm motility disorders (Sha et al., 2014). Thus, axoneme structures are very important to sperm morphology and the function of the flagellum.

The 'multiple morphological abnormalities of the flagella' (MMAF) phenotype is a severe teratozoospermia (Coutton et al., 2015) that is characterized by various spermatozoa phenotypes with absent, short, coiled or irregular flagella. Many flagellar axoneme defects exist in individuals with MMAF, including disrupted microtubule doublets, ODFs, FSs, outer or inner dynein arms and others (Jiao et al., 2021). Over the past several years, many mutations have been found to be associated with MMAF individuals, and many mouse models display MMAF-like phenotypes, such as those containing loss-of-function mutants for *Dnah2* (Li et al., 2019), *Dnah8* (Liu et al., 2020), *Cfap44*, *Cfap65* (Tang et al., 2017; Li et al., 2020), *Qrich2* (Shen et al., 2019), *Cep135* (Sha et al., 2017) and *Ttc21a* (Liu et al., 2019), all of which have been reported as MMAF-related genes. Despite rapid progress having been made in understanding the mechanisms underlying MMAF, the pathogenesis associated with human idiopathic MMAF remains unknown.

Coiled-coil domain-containing (CCDC) proteins are involved in a variety of physiological and pathological processes. An increasing number of CCDC proteins have been suggested to be involved in ciliogenesis (Priyanka and Yenugu, 2021), yet only some of those genes are involved in spermatogenesis, such as *Ccdc9*, *Ccdc11*, *Ccdc33*, *Ccdc42*, *Ccdc63* and *Ccdc172*. These genes are associated with sperm flagellum biogenesis and manchette formation, and their defects lead to male infertility (Sha et al., 2019; Wu et al., 2021; Tapia Contreras and Hoyer-Fender, 2019; Young et al., 2015; Yamaguchi et al., 2014). CCDC42 is a highly expressed protein in mouse testis, and localizes to the manchette, head-to-tail coupling apparatus (HTCA) and sperm tail during spermatogenesis. CCDC42 is necessary for HTCA assembly and sperm flagellum biogenesis (Tapia Contreras and Hoyer-Fender, 2019); however, the functional role of CCDC42 in spermatogenesis is still not understood.

Here, we find that CCDC38 interacts with CCDC42, is highly expressed in the testis and associates with the manchette in the elongating spermatid. Importantly, *Ccdc38* knockout in mice resulted

[1]State Key Laboratory of Stem Cell and Reproductive Biology, Institute of Zoology, Stem Cell and Regenerative Medicine Innovation Institute, Chinese Academy of Sciences, Beijing 100101, China. [2]Institute of Reproductive Health and Perinatology, Guangzhou Women and Children's Medical Center, Guangzhou Medical University, Guangzhou 510623, China. [3]University of the Chinese Academy of Sciences, Beijing 100049, China. [4]Department of Urology, Peking University Third Hospital, Beijing 100191, China. [5]Department of Andrology, Peking University Third Hospital, Beijing 100191, China. [6]Department of Reproductive Medicine Center, Peking University Third Hospital, Beijing 100191, China. [7]Department of Human Sperm Bank, Peking University Third Hospital, Beijing 100191, China. [8]Savaid Medical School, University of Chinese Academy of Sciences, Beijing 100049, China.
*These authors contributed equally to this work

‡Authors for correspondence (leways@gwcmc.org; yuanli@ucas.ac.cn; gaof@ioz.ac.cn; jianghui55@163.com)

R.Z., 0000-0002-4924-8766; B.W., 0000-0001-9269-4414; X.W., 0000-0002-2268-4680; Y.C., 0000-0003-2169-4673; H.W., 0000-0002-8087-0262; H.J., 0000-0002-6256-2733; F.G., 0000-0003-4415-6165; L.Y., 0000-0002-1816-5618; W.L., 0000-0002-6235-0749

Handling Editor: Haruhiko Koseki
Received 11 January 2022; Accepted 14 April 2022

Development (2022) 149, dev200516. doi:10.1242/dev.200516

in an abnormally elongated manchette and an MMAF-like phenotype. Furthermore, we find that CCDC38 interacts with the proteins intraflagellar transport 88 (IFT88) and ODF2 to facilitate ODF2 transport in the flagellum. Our results suggest that the CCDC42-CCDC38 interaction mediates ODF2 transport during flagellum biogenesis, and both proteins are essential for flagellum biogenesis and fertility in male mice, suggesting mutations of these two genes might be associated with male infertility in humans.

RESULTS

CCDC38 interacts with CCDC42

Many CCDC proteins participate in flagellum biogenesis during spermiogenesis (Priyanka and Yenugu, 2021). CCDC42 localizes to the centrosome, HTCA, manchette and sperm tail in male germ cells, and it is involved in the biogenesis of motile cilia and flagella in mice (Perles et al., 2012; Tapia Contreras and Hoyer-Fender, 2019; Pasek et al., 2016; Silva et al., 2016). To understand the underlying mechanism of CCDC42 in flagellum biogenesis during spermiogenesis, we used the Search Tool for the Retrieval of Interacting Genes/Proteins (STRING) database to search for CCDC42-binding candidates (Fig. 1A), and chose to analyze the role of CCDC38, which is exclusively expressed in testes (Lin et al., 2016). Epitope-tagged CCDC42 and CCDC38 were expressed in human embryonic kidney 293 expressing SV40 large T antigen (HEK293T) cells and followed by immunoprecipitation experiments using the anti-MYC antibody, which demonstrated that CCDC38 co-immunoprecipitated with CCDC42 (Fig. 1B). An overlapping immunostaining pattern was clearly seen in HeLa cells transiently expressing GFP-CCDC38 and MYC-CCDC42 and GFP-CCDC38 also colocalized with γ-tubulin as reported (Firat-Karalar et al., 2014) (Fig. 1C; Fig. S1). These results suggest that CCDC42 can indeed interact with CCDC38.

Next, we examined the localization of endogenous CCDC38 during spermatogenesis. CCDC38 was detected as two adjacent spots near the nuclei of spermatocytes or round spermatids, and it localized to the skirt-like structure encircling the spermatid head from steps 9 to 14 (Lehti and Sironen, 2016) and the testicular sperm tail (Fig. 1D). We, therefore, speculate that CCDC38 might participate in flagellum biogenesis during spermiogenesis.

Ccdc38 knockout leads to male infertility

Reverse transcription PCR (RT-PCR) analysis detected *Ccdc38* expression in the testis and revealed that *Ccdc38* was first expressed at postnatal day (P) 14, peaking at P35 (Fig. 2A,B). To determine the physiological role of CCDC38, we generated *Ccdc38*-deficient mice using the CRISPR/Cas9 system to delete exons 5-11 of the *Ccdc38* gene (Fig. 2C). The *Ccdc38*-knockout mice were genotyped by genomic DNA sequencing and further confirmed

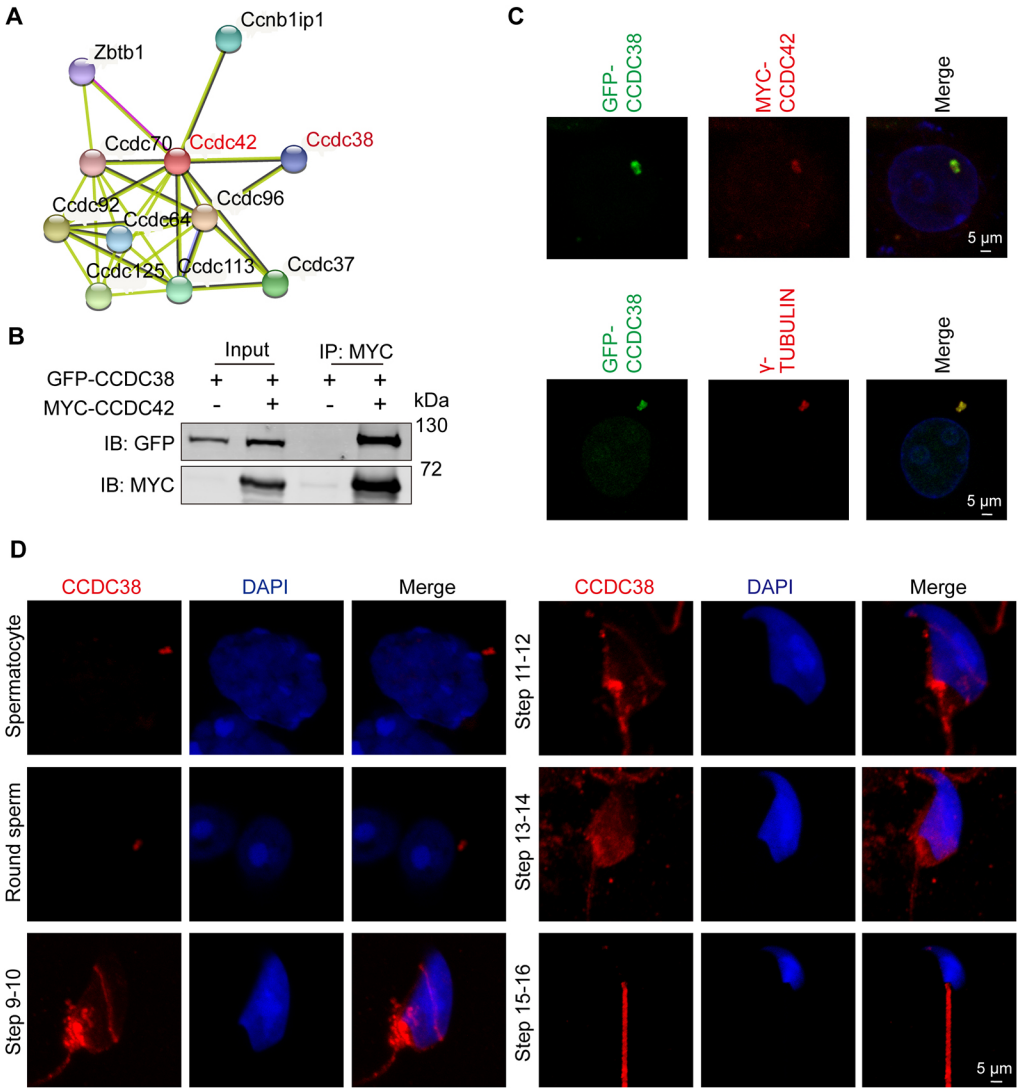

Fig. 1. CCDC38 interacts with CCDC42. (A) CCDC38 might interact with CCDC42 as predicted by the STRING database. (B) CCDC38 immunoprecipitated with CCDC42. pCSII-MYC-CCDC42 and pEGFP-C1-CCDC38 plasmids were transfected into HEK293T cells. Forty-eight hours after transfection, cell lysates were collected for immunoprecipitation with the anti-MYC antibody, and the immunoprecipitates were detected using anti-MYC or anti-GFP antibodies. IB, immunoblotting; IP, immunoprecipitation. (C) CCDC38 colocalized with CCDC42 and γ-tubulin in HeLa cells. pCSII-MYC-CCDC42 and pEGFP-C1-CCDC38 plasmids were co-transfected into HeLa cells. 48 h after transfection, the cells were fixed and stained with anti-MYC and anti-γ-tubulin antibodies, and the nuclei were stained with DAPI (blue). (D) Testicular germ cells were stained using the anti-CCDC38 antibody, and the nuclei were stained with DAPI. Scale bars: 5 μm. Images are representative of five experiments.

Development (2022) 149, dev200516. doi:10.1242/dev.200516

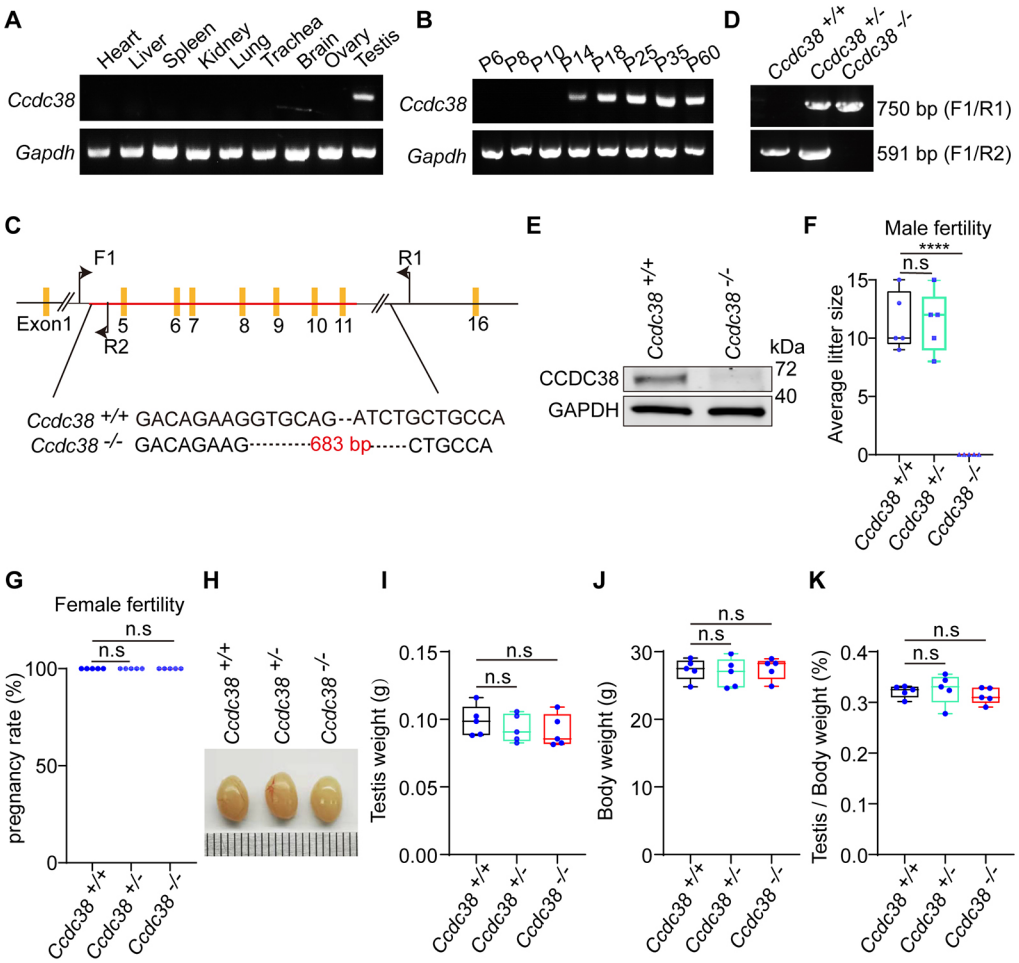

Fig. 2. *Ccdc38* knockout leads to male infertility. (A) RT-PCR analysis of the expression of *Ccdc38* in different tissues. (B) RT-PCR analysis of the expression of *Ccdc38* on different days after birth. (C) Schematic showing the generation of *Ccdc38*$^{-/-}$ mice lacking exons 5-11. (D) Genotyping of *Ccdc38*$^{+/+}$, *Ccdc38*$^{+/-}$ and *Ccdc38*$^{-/-}$ mice. In A,B,D, *Gapdh* was used as an internal control. (E) Western blot for CCDC38 to show the efficiency of CCDC38 depletion in *Ccdc38*$^{-/-}$ male mice. GAPDH was used as a loading control. Images are representative of three experiments. (F) The average litter sizes of *Ccdc38*$^{+/+}$, *Ccdc38*$^{+/-}$ and *Ccdc38*$^{-/-}$ mice at 2 months. No pregnancy occurred in females mated with *Ccdc38*$^{-/-}$ male mice. (G) Pregnancy rates of *Ccdc38*$^{+/+}$, *Ccdc38*$^{+/-}$ and *Ccdc38*$^{-/-}$ female mice at 2 months. No obvious differences were observed between *Ccdc38*$^{+/+}$, *Ccdc38*$^{+/-}$ and *Ccdc38*$^{-/-}$ mice. (H) The sizes of the testes from *Ccdc38*$^{+/-}$ and *Ccdc38*$^{-/-}$ mice were not affected compared with those from *Ccdc38*$^{+/+}$ mice. (I) Testes from *Ccdc38*$^{+/+}$, *Ccdc38*$^{+/-}$ and *Ccdc38*$^{-/-}$ male mice showed no obvious differences in weight (n=5). (J) The body weights of *Ccdc38*$^{+/+}$, *Ccdc38*$^{+/-}$ and *Ccdc38*$^{-/-}$ male mice showed no obvious differences (n=5). (K) The ratios of testis/body weight in *Ccdc38*$^{+/+}$, *Ccdc38*$^{+/-}$ and *Ccdc38*$^{-/-}$ male mice were not significantly different (n=5). For box plots, the box represents the 25-75th percentiles, the central line indicates the median and the whiskers show the minimum to maximum values, with each individual value as point in the graph. n.s., not significant; ****P<0.0001 (paired two-tailed Student's t-test).

by PCR, as seen by the 591 bp band for the wild-type (WT) allele, 750 bp band for homozygotes, and two bands of 750 bp and 591 bp for heterozygotes (Fig. 2D). Subsequent western blotting analysis validated complete ablation of CCDC38 in the total protein extracts from *Ccdc38*$^{-/-}$ testes (Fig. 2E). We next examined the fertility of *Ccdc38*$^{+/+}$, *Ccdc38*$^{+/-}$ and *Ccdc38*$^{-/-}$ mice. Male *Ccdc38*$^{-/-}$ mice exhibited normal mounting behaviors and produced coital plugs but failed to produce any offspring after mating with WT adult female mice (Fig. 2F). In contrast, female *Ccdc38*$^{-/-}$ mice could generate offspring after mating with WT adult males, similar to the *Ccdc38*$^{+/+}$ female mice (Fig. 2G). However, the knockout of *Ccdc38* did not affect either testis size (Fig. 2H) or the ratio of testis weight to body weight (Fig. 2I-K). Taken together, *Ccdc38* knockout leads to male infertility.

Ccdc38 knockout results in MMAF

To explore the cause of male infertility further, we examined the cauda epididymis of *Ccdc38*$^{+/+}$, *Ccdc38*$^{+/-}$ and *Ccdc38*$^{-/-}$ mice by Hematoxylin and Eosin (H&E) staining, and found fewer spermatozoa in the epididymal lumen of *Ccdc38*$^{-/-}$ mice compared with *Ccdc38*$^{+/+}$ and *Ccdc38*$^{+/-}$ mice (Fig. 3A). We next released spermatozoa from the epididymis and found that the number of sperm from *Ccdc38*$^{-/-}$ mice was significantly less than that of *Ccdc38*$^{+/+}$ and *Ccdc38*$^{+/-}$ mice (Fig. 3B). The percentage of spermatozoa that were motile decreased sharply for *Ccdc38*$^{-/-}$ mice compared with *Ccdc38*$^{+/+}$ and *Ccdc38*$^{+/-}$ mice (Fig. 3C), but sperm number and motility showed no obvious differences between *Ccdc38*$^{+/+}$ and *Ccdc38*$^{+/-}$ mice (Fig. 3B,C). Thus, we focused our attention on only *Ccdc38*$^{+/+}$ and *Ccdc38*$^{-/-}$ mice in subsequent studies. We also noticed that *Ccdc38*$^{-/-}$ spermatozoa showed morphological aberrations, including abnormal nuclei and an MMAF-like phenotype of either a short tail (type 1), disordered filaments (type 2), impaired spermatozoon head (type 3), curly tail (type 4) and tailless (type 5) (Fig. 3D). The percentage of spermatozoa with abnormal heads and flagella is shown in Fig. 3E. Scanning electron microscopy (SEM) further revealed the

Development (2022) 149, dev200516. doi:10.1242/dev.200516

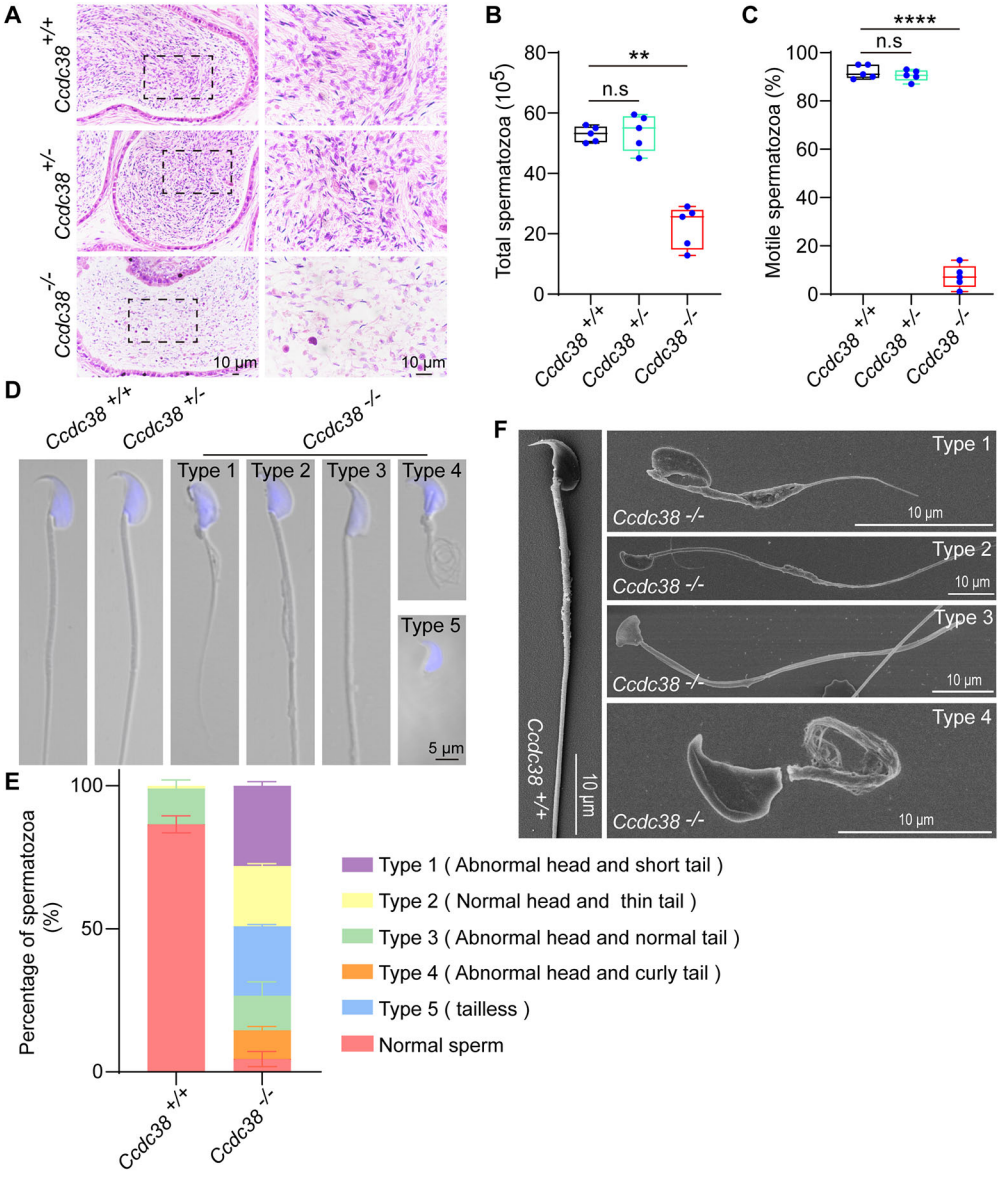

Fig. 3. *Ccdc38* knockout results in MMAF. (A) H&E staining of the caudal epididymis. Magnified images (dashed boxes) are shown on the right. (B) Sperm number obtained from *Ccdc38*$^{+/+}$, *Ccdc38*$^{+/-}$ and *Ccdc38*$^{-/-}$ mice (n=5). (C) The percentage of motile spermatozoa from *Ccdc38*$^{+/+}$, *Ccdc38*$^{+/-}$ and *Ccdc38*$^{-/-}$ mice (n=5). For box plots, the box represents the 25-75th percentiles, the central line indicates the median and the whiskers show the minimum to maximum values. n.s., not significant; **P<0.01; ****P<0.0001 (paired two-tailed Student's t-test). (D) For single-sperm immunofluorescence analysis of *Ccdc38*$^{+/+}$, *Ccdc38*$^{+/-}$ and *Ccdc38*$^{-/-}$ mice, the nucleus was stained with DAPI and five sperm phenotypes were observed: short tail (type 1), disordered tail (type 2), abnormal nuclei (type 3), curly tail (type 4) and tailless (type 5). (E) The percentages of different spermatozoa observed in *Ccdc38*$^{+/+}$ and *Ccdc38*$^{-/-}$ caudal epididymides. Data are presented as the mean±s.d. (F) SEM analysis of spermatozoa from the epididymides of *Ccdc38*$^{+/+}$ and *Ccdc38*$^{-/-}$ mice. Morphological abnormalities were seen in types 1-4 for *Ccdc38*$^{-/-}$ sperm compared with *Ccdc38*$^{+/+}$ sperm. Images are representative of five experiments. Scale bars: 10 μm (A,F); 5 μm (D).

morphological abnormalities of *Ccdc38*$^{-/-}$ spermatozoa (Fig. 3F). Therefore, the knockout of *Ccdc38* results in an MMAF-like phenotype in mice.

Spermiogenesis is impaired in *Ccdc38*$^{-/-}$ mice

To investigate further why *Ccdc38* knockout led to an MMAF-like phenotype, we first used Periodic acid-Schiff (PAS) staining to determine in which stages the defects occurred. During spermatogenesis, the cycle of the seminiferous epithelium can be subdivided into 12 stages, which can be distinguished from one another by steps in spermatid development. Meanwhile, the spermatid development can be subdivided into 16 steps, according to acrosome and sperm nuclear morphology (Griswold et al., 2016). In testis sections from *Ccdc38*$^{+/+}$ mice, round spermatids differentiated into elongating spermatids from stage IX (Griswold et al., 2016), whereas abnormal elongated spermatids occurred at stage X in the testes of *Ccdc38*$^{-/-}$ mice (Fig. 4A). To delineate the detailed defects of *Ccdc38*$^{-/-}$ spermatids, we analyzed steps 1-16 for spermiogenesis in both *Ccdc38*$^{+/+}$ and *Ccdc38*$^{-/-}$ mice, and found that at steps 1-8, the morphology of acrosomes and nuclei of *Ccdc38*$^{-/-}$ spermatids was similar to that of *Ccdc38*$^{+/+}$ spermatids. In *Ccdc38*$^{+/+}$ mice, spermatid head elongation and maturation began at step 9, whereas in *Ccdc38*$^{-/-}$ mice, spermatid head elongation and maturation showed abnormalities at step 9, eventually leading to abnormal spermatozoa at step 16 (Fig. 4B). These results support the hypothesis that CCDC38 plays an essential role during spermiogenesis.

The flagellum is disorganized and the manchette is ectopically placed in *Ccdc38*$^{-/-}$ spermatids

To study the causes of abnormal sperm morphology after *Ccdc38* depletion, H&E staining was used to determine the morphology of seminiferous tubules in *Ccdc38*$^{+/+}$ and *Ccdc38*$^{-/-}$ mice. Compared with *Ccdc38*$^{+/+}$ testes, obvious shortened tails and tailless spermatids could be detected in *Ccdc38*$^{-/-}$ testes (Fig. 5A). Immunofluorescence staining for the flagellum marker acetylated tubulin (Ac-tubulin) further confirmed the flagellum biogenesis defects in *Ccdc38*$^{-/-}$ testes (Fig. 5B). We conducted

Development (2022) 149, dev200516. doi:10.1242/dev.200516

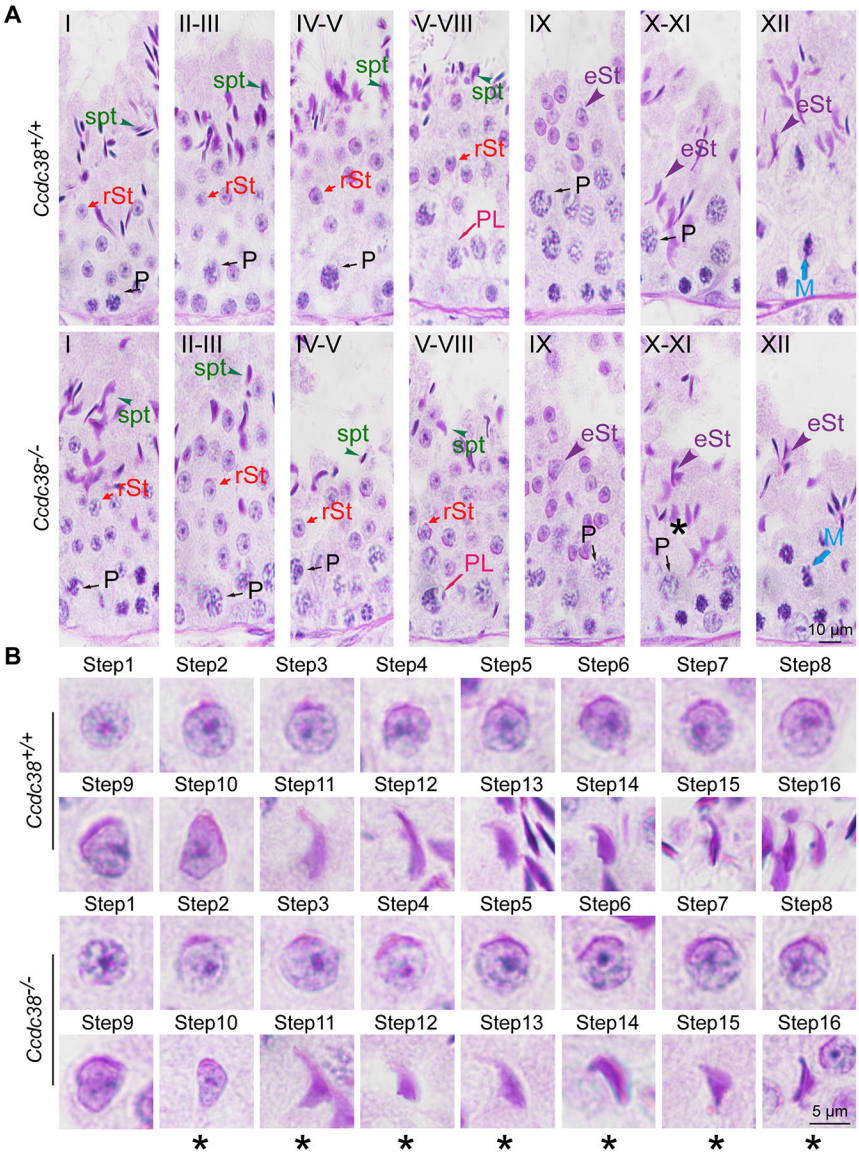

Fig. 4. Spermiogenesis is impaired in *Ccdc38*$^{-/-}$ mice. (A) PAS staining of *Ccdc38*$^{-/-}$ testis sections showed abnormal sperm nuclear shape. eSt, elongating spermatid; M, meiotic spermatocyte; P, pachytene; PL, pre-leptotene spermatocyte; rSt, round spermatid; spt, spermatozoa. The asterisk indicates an abnormal elongated spermatid at stages X-XI in *Ccdc38*$^{-/-}$ mice. (B) PAS staining of spermatids at different steps from *Ccdc38*$^{+/+}$ and *Ccdc38*$^{-/-}$ mice. Asterisks indicate abnormal spermatid shapes found starting at step 10. Images are representative of five experiments. Scale bars: 10 µm (A); 5 µm (B).

immunofluorescence analysis of lectin peanut agglutinin (PNA) which marks the acrosome, and Ac-tubulin to determine which stages were affected by *Ccdc38* knockout and found that the flagella of *Ccdc38*$^{-/-}$ spermatids were short and curly from stages IV-V compared with those of *Ccdc38*$^{+/+}$ spermatids (Fig. 5C). Using transmission electron microscopy (TEM), we observed that the ODFs, FS, mitochondrial sheath and axoneme were also abnormally organized in the *Ccdc38*$^{-/-}$ elongating spermatids (Fig. 5D).

When spermatids were elongated, the sperm head was found to be abnormal in the *Ccdc38*$^{-/-}$ spermatids, indicating that the manchette might be abnormally formed (stage X-XI, Fig. 5C). The manchette is important for sperm head shaping (Wei and Yang, 2018), so we turned our attention to evaluating manchette structure. We found the manchettes of *Ccdc38*$^{-/-}$ spermatids were roughly normal at steps 8-10 but were abnormally longer at steps 11-12 compared with control spermatids (Fig. 6A). We also used TEM to analyze the manchette in further detail and found *Ccdc38*$^{-/-}$ spermatids, but not *Ccdc38*$^{+/+}$ spermatids, became abnormally elongated at step 11 (Fig. 6B). In support of these results, we found that CCDC38 colocalized with α-tubulin to the manchette in control mice (Fig. 6C). All these results suggest that CCDC38 is directly involved in flagellum biogenesis.

CCDC38 interacts with IFT88

It has been reported that CCDC42, IFT88, CFAP53 and KIF3A are involved in anterograde transport during flagellum biogenesis (Wu et al., 2021). To test whether CCDC38 also participates in anterograde transport by interacting with CFAP53 and intraflagellar transport (IFT) complexes, such as IFT88 and IFT20, we co-transfected pCSII-MYC-IFT88, pCSII-MYC-CFAP53 or pRK-FLAG-IFT20 with pEGFP-C1-CCDC38 in HEK293T cells. We next immunoprecipitated CCDC38 using the anti-GFP antibody and found that IFT88 and CFAP53, but not IFT20, immunoprecipitated with CCDC38 (Fig. 7A-C). We also analyzed protein expression levels in *Ccdc38*$^{+/+}$ and *Ccdc38*$^{-/-}$ mice testes and found that IFT88, CFAP53 and IFT20 expression levels were all significantly decreased in *Ccdc38*$^{-/-}$ mice testes compared with *Ccdc38*$^{+/+}$ mice testes (Fig. 7D,E). Because IFT88 can participate in anterograde transport, we next evaluated the distribution of IFT88 in spermatids at different steps and found that

Development (2022) 149, dev200516. doi:10.1242/dev.200516

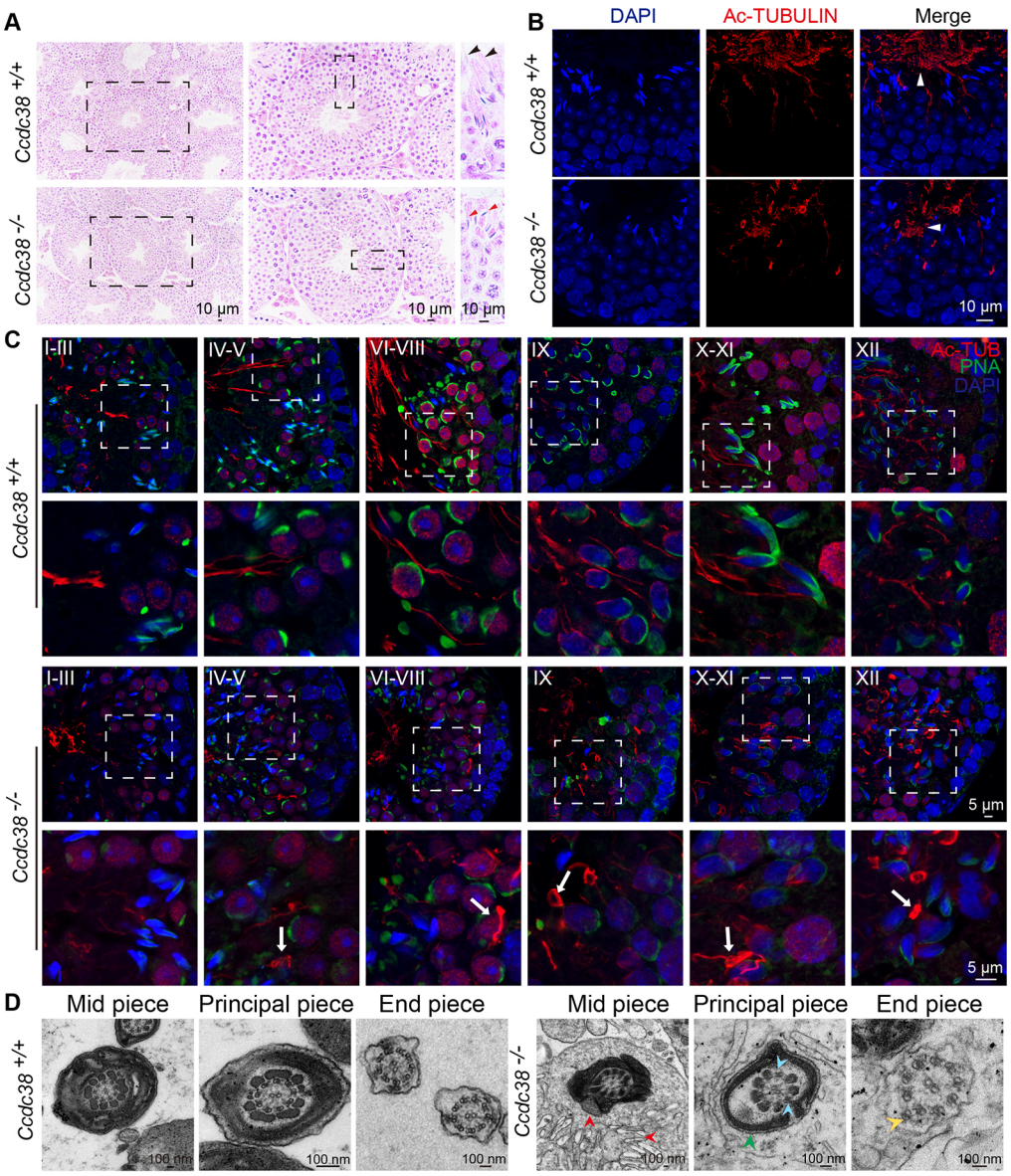

Fig. 5. The flagellum is disorganized in *Ccdc38*$^{-/-}$ spermatids. (A) Histology of the seminiferous tubules from *Ccdc38*$^{+/+}$ and *Ccdc38*$^{-/-}$ male mice. Black arrowheads indicate normal sperm tails in the *Ccdc38*$^{+/+}$ testis seminiferous tubule, red arrowheads indicate the abnormal sperm flagellum in the *Ccdc38*$^{-/-}$ testis seminiferous tubule. Dashed boxes indicate the areas shown at higher magnification to the right. (B) Immunofluorescence analysis for Ac-tubulin (red) in *Ccdc38*$^{-/-}$ mice testes showed flagellar defects. The nucleus was stained with DAPI (blue). White arrowheads indicate sperm flagella in *Ccdc38*$^{+/+}$ and *Ccdc38*$^{-/-}$ mice. (C) Immunofluorescence analysis for Ac-tubulin (red) and lectin PNA (green) to identify sperm flagellum biogenesis. Magnified images (dashed boxes) are shown in the lower panels. White arrows indicate short tails that were found from stages IV-V in *Ccdc38*$^{-/-}$ mice compared with the control group. (D) Cross-sections of *Ccdc38*$^{-/-}$ sperm tails revealed the disorganization of axonemal microtubules and tail accessory structures. Red arrowheads indicate abnormal mitochondria and the cytoplasm, blue arrowheads indicate the loss of outer dense fibers, the green arrowhead indicates the abnormal fibrous sheath, and the yellow arrowhead indicates an abnormal axoneme. Images are representative of three experiments. Scale bars: 10 μm (A,B); 5 μm (C); 100 nm (D).

IFT88 was present in the manchette and elongating sperm tails in *Ccdc38*$^{+/+}$ mice, whereas in the *Ccdc38*$^{-/-}$ spermatids, IFT88 also localized to the manchette and elongating sperm tails in spermatids (Fig. 7F). Therefore, CCDC38 might regulate sperm flagellum biogenesis by interacting with IFT88.

ODF2 transportation is impaired in *Ccdc38*-knockout spermatids

It has been reported that ODF1 and ODF2 can interact with CCDC42 and have been found to be involved in the formation of the male germ cell cytoskeleton (Tapia Contreras and Hoyer-Fender, 2019). To study the relationship between CCDC38 and ODF2, reciprocal co-immunoprecipitation assays were carried out. We transfected the pCDNA-HA-ODF2 and pEGFP-C1-CCDC38 plasmids into HEK293T cells and found that CCDC38 and ODF2 were able to immunoprecipitate with each other (Fig. 8A). These findings suggest that CCDC38 interacts with ODF2.

As the main scaffolding protein in ODFs, ODF2 is essential for sperm flagellum integrity and beating (Donkor et al., 2004; Ito et al., 2019; Fawcett, 1975). To determine the effects of *Ccdc38* knockout on ODF1 and ODF2 protein levels, we examined testicular extracts and found that ODF2, but not ODF1, levels were significantly decreased in *Ccdc38*$^{-/-}$ testicular extracts (Fig. 8B,C) compared with those of *Ccdc38*$^{+/+}$. Next, we used immunofluorescence to analyze the localization of ODF2 in spermatids and epididymal spermatozoa. We found that ODF2 localized on the manchette, along with the sperm tail, in elongated spermatids of *Ccdc38*$^{+/+}$ mice, whereas it localized on the manchette without tail staining in most of the elongated spermatids of *Ccdc38*$^{-/-}$ mice (Fig. 8D). Of note, ODF2 colocalized with α-tubulin in the midpiece and principal piece of *Ccdc38*$^{+/+}$ sperm tails, whereas it displayed discontinuous, punctiform signals in only short or curly tails in *Ccdc38*-knockout spermatozoa (Fig. 8E), suggesting that ODF defects in *Ccdc38*-knockout spermatozoa might arise from ODF2 transport defects during spermiogenesis.

DISCUSSION

Ccdc38 is exclusively expressed in testes (Lin et al., 2016), but its role during spermiogenesis has not yet been investigated. To study its role during spermiogenesis, we generated a *Ccdc38*$^{-/-}$ mouse

Development (2022) 149, dev200516. doi:10.1242/dev.200516

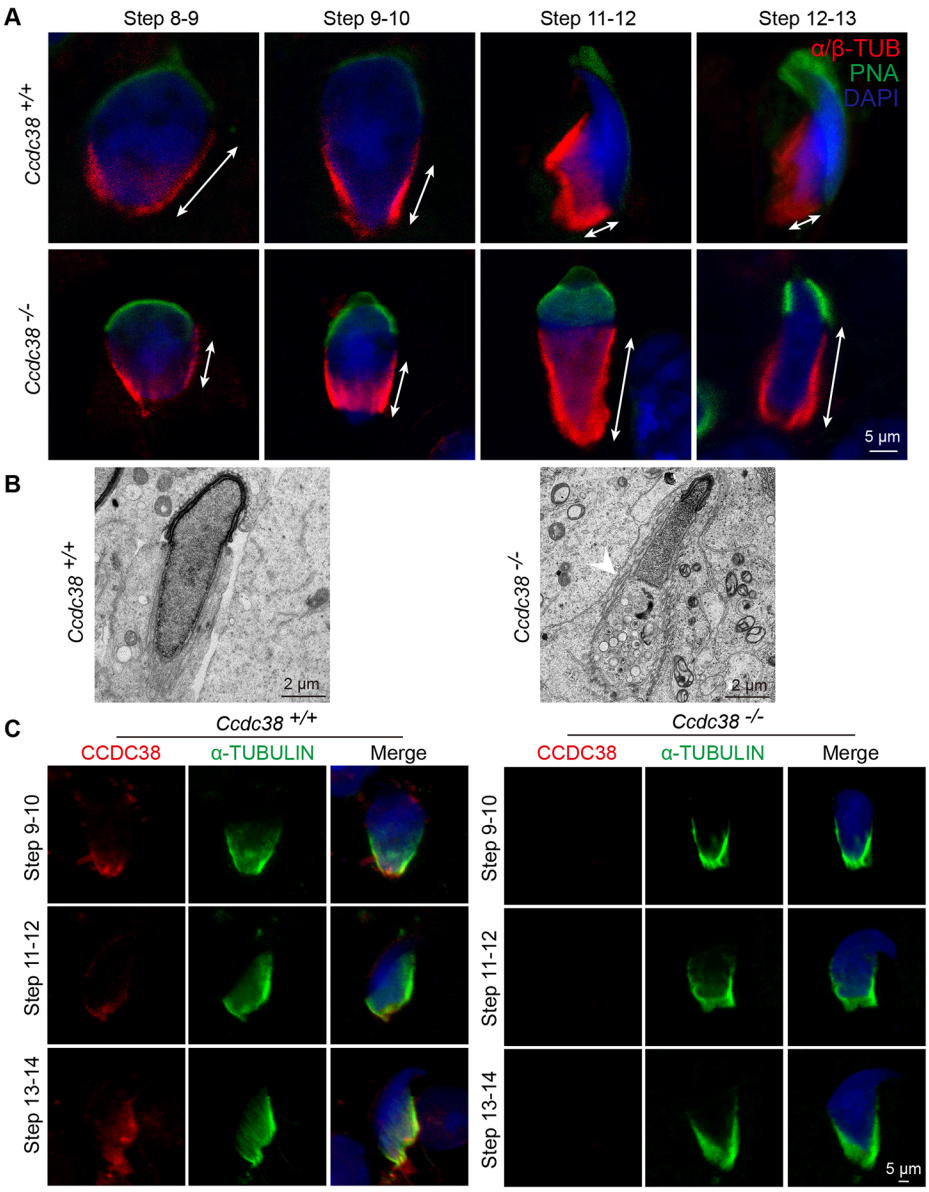

Fig. 6. The manchette is ectopically placed in *Ccdc38*$^{-/-}$ spermatids. (A) Abnormal manchette elongation in *Ccdc38*$^{-/-}$ spermatids. Spermatids from different manchette-containing steps were stained with antibodies against α/β-tubulin (red) and lectin PNA (green, acrosome marker) to visualize the manchette (double-headed arrows). *Ccdc38*$^{-/-}$ spermatids displayed abnormal elongation of the manchette. (B) TEM revealed that the manchette of elongating spermatids (steps 9-11) from *Ccdc38*$^{-/-}$ mice were ectopically placed. The white arrowhead indicates the abnormal manchette. (C) Localization of CCDC38 during different germ-cell stages. Immunofluorescence of CCDC38 and α-tubulin in developing germ cells. The manchette was stained with the anti-α-tubulin antibody, and nuclei were stained with DAPI. Images are representative of five experiments. Scale bars: 5 μm (A,C); 2 μm (B).

model and found *Ccdc38*$^{-/-}$ male mice to be sterile (Fig. 2F) owing to significantly reduced spermatozoa number and motility (Fig. 3B,C). As for which kinds of cells were affected by CCDC38 function, a discrepancy exists between our results and others. Lin et al. (2016) previously reported that CCDC38 is mainly localized to spermatogonia and spermatocytes, but we found that CCDC38 mainly participates in spermatid elongation and is localized on the manchette and the sperm tail (Fig. 1D, Fig. 6C). The discrepancy may have arisen from different CCDC38 antibodies being used. Our CCDC38 antibody was validated by both western blotting (Fig. 2E) and immunofluorescence (Fig. 6C), supporting the robustness of our antibody labeling and the findings of our protein localization in this study. Further support for the manchette and sperm tail localization of CCDC38 is shown by the knockout of *Ccdc38*, which results in MMAF but does not affect ciliogenesis in the lung and trachea of *Ccdc38*$^{-/-}$ mice (Fig. S2). These results suggest that CCDC38 could be directly involved in flagellum biogenesis but not in other processes.

The manchette is a transient structure in developing germ cells, which is required for sperm nuclear condensation and flagellum biogenesis (Wei and Yang, 2018) by providing the structural basis for intra-manchette transport (IMT). IMT transfers structural and functional proteins to the basal body and is essential for nucleocytoplasmic transport (Kierszenbaum, 2002; Kierszenbaum et al., 2002). As an IMT component, CCDC42 localizes to the manchette, connecting piece, and sperm tail during spermiogenesis, and can interact with ODF1 and ODF2 to regulate germ cell cytoskeleton formation (Tapia Contreras and Hoyer-Fender, 2019; Pasek et al., 2016). In this study, we found that CCDC38 interacts with CCDC42, colocalizes with CCDC42 on centrosomes in HeLa cells (Fig. 1A-C) and interacts with ODF2 and ODF1 (Fig. 8A; Fig. S3). Both ODF1 and ODF2 are components of ODFs and are important for male fertility. The knockout of *Odf1* in mice impairs sperm head-to-tail coupling (Yang et al., 2014, 2012), whereas the knockout of *Odf2* leads to pre-implantation lethality. Even the absence of a single copy of this gene results in separation of the sperm neck and midpiece (Qian et al., 2016; Tarnasky et al., 2010). Furthermore, recent human infertility studies showed that mutations in *ODF2* caused MMAF (Zhu et al., 2022). Consistent with the clinical studies, we found that in *Ccdc38*-knockout mice, ODF2 but

Development (2022) 149, dev200516. doi:10.1242/dev.200516

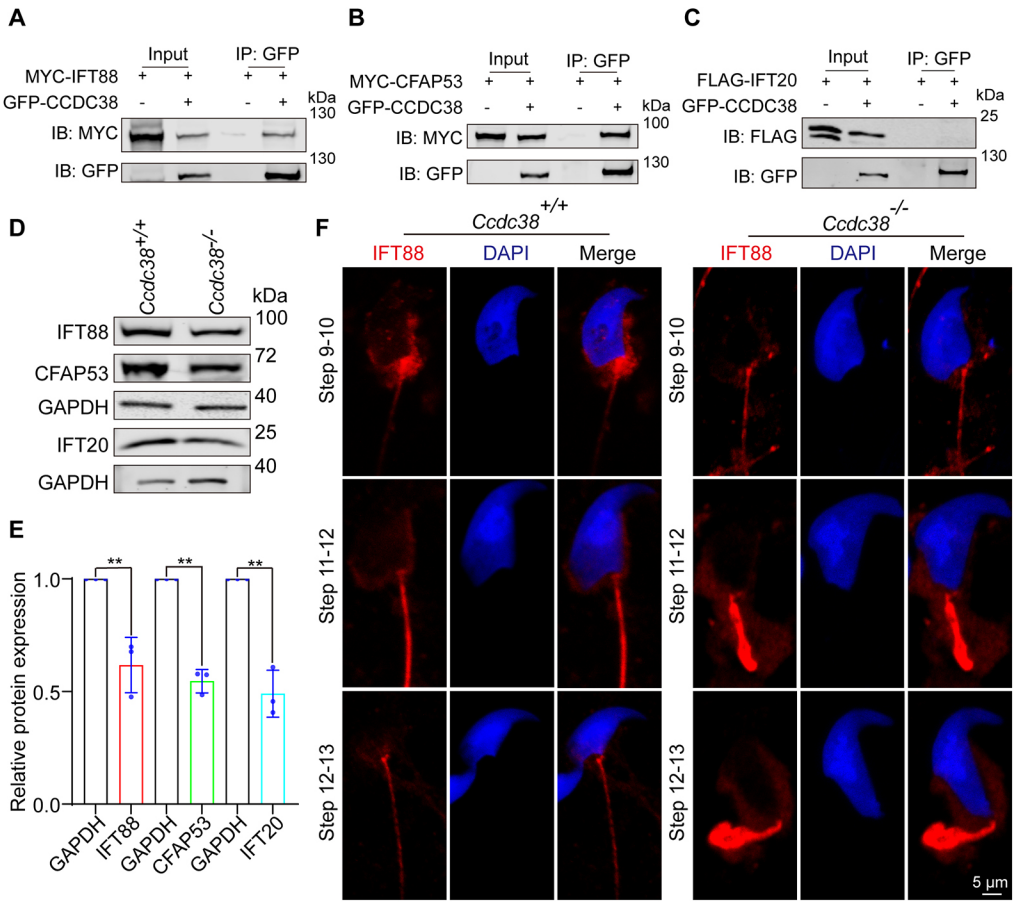

Fig. 7. CCDC38 interacts with IFT88 and CFAP53, but not IFT20. (A) IFT88 immunoprecipitated with CCDC38. pCSII-MYC-IFT88 and pEGFP-C1-CCDC38 plasmids were transfected into HEK293T cells. 48 h after transfection, cell lysates were collected for immunoprecipitation with the anti-GFP antibody, and analyzed using the anti-MYC or anti-GFP antibodies. IB, immunoblotting; IP, immunoprecipitation. (B) CCDC38 interacted with CFAP53. pCSII-MYC-CFAP53 and pEGFP-C1-CCDC38 plasmids were transfected into HEK293T cells. 48 h after transfection, cell lysates were collected for immunoprecipitation using the anti-GFP antibody, and analyzed with the anti-MYC or anti-GFP antibodies. (C) CCDC38 did not interact with IFT20. pRK-FLAG-IFT20 and pEGFP-C1-CCDC38 plasmids were transfected into HEK293T cells. 48 h after transfection, cell lysates were collected for immunoprecipitation with the anti-GFP antibody, and analyzed using the anti-FLAG or anti-GFP antibodies. (D) Western blots showing IFT88, CFAP53 and IFT20 protein levels in lysates from *Ccdc38*$^{+/+}$ and *Ccdc38*$^{-/-}$ mice testes. GAPDH served as a loading control. The two blots for GAPDH represent two independent experiments. (E) Quantitative results of western blotting. Protein levels were normalized against GAPDH levels. Data are presented as the mean±s.d. $^{**}P<0.01$ (paired two-tailed Student's *t*-test). (F) Immunofluorescence of IFT88 (red) and DAPI (blue) in different spermatid stages in *Ccdc38*$^{+/+}$ and *Ccdc38*$^{-/-}$ mice. Images are representative of five experiments. Scale bars: 5 µm.

not ODF1 protein levels decreased in the testis (Fig. 8B,C) and ODF2 distribution was altered in flagella (Fig. 8D,E). Thus, CCDC38 either works as a partner of ODF2 to support its stability or participates in IMT to mediate ODF2 transport during flagellum biogenesis. As CCDC38 also interacted with CCDC42, we believe CCDC38 plays a role in ODF2 transport, and this is further supported by its interaction with IFT88.

In addition to IMT, IFT is also required for flagellum biogenesis, and is responsible for protein transport during the development of the flagellum. During IFT, various cargos are transported from the basal body to the tip of the flagellum and then back to the sperm head along the axoneme (Scholey, 2003; Taschner and Lorentzen, 2016; Ishikawa and Marshall, 2017). IFT88 is a component of the IFT-B complex and is present only in the heads and tails of elongating spermatids, and not in mature sperm (San Agustin et al., 2015). IFT88 has been found to interact with KIF3B to regulate anterograde transport along the axoneme (Rosenbaum and Witman, 2002; Funabashi et al., 2018). As an IFT88-interacting protein (Fig. 7A), CCDC38 may also participate in anterograde transport along the flagellum. Previously, we found that CFAP53 could interact with both CCDC42 and IFT88 to regulate the anterograde transport along the flagellum (Wu et al., 2021). In this study, we found that CCDC38 also interacts with CFAP53 (Fig. 7B). Thus, through its interactions with CFAP53, CCDC42 and IFT88, CCDC38 may regulate cargo transport by IMT and IFT during flagellum biogenesis. Further investigations are needed to reveal the detailed roles of these proteins and their relationships during flagellum biogenesis.

In summary, we have identified a new CCDC42-interacting protein, CCDC38, that is essential for spermiogenesis and flagellum biogenesis, as the knockout of *Ccdc38* results in an MMAF-like phenotype in mice. Given that these genes are evolutionarily conserved in humans, we believe that mutations of these genes may exist in individuals with MMAF and further studies should be undertaken to uncover how these mutations affect disease presentation.

MATERIALS AND METHODS

Plasmids

Mouse *Ccdc42*, *Cfap53* and *Ift88* were obtained from mouse testis cDNA and were cloned into the pCSII-Myc vector using the Clone Express Ultra

Development (2022) 149, dev200516. doi:10.1242/dev.200516

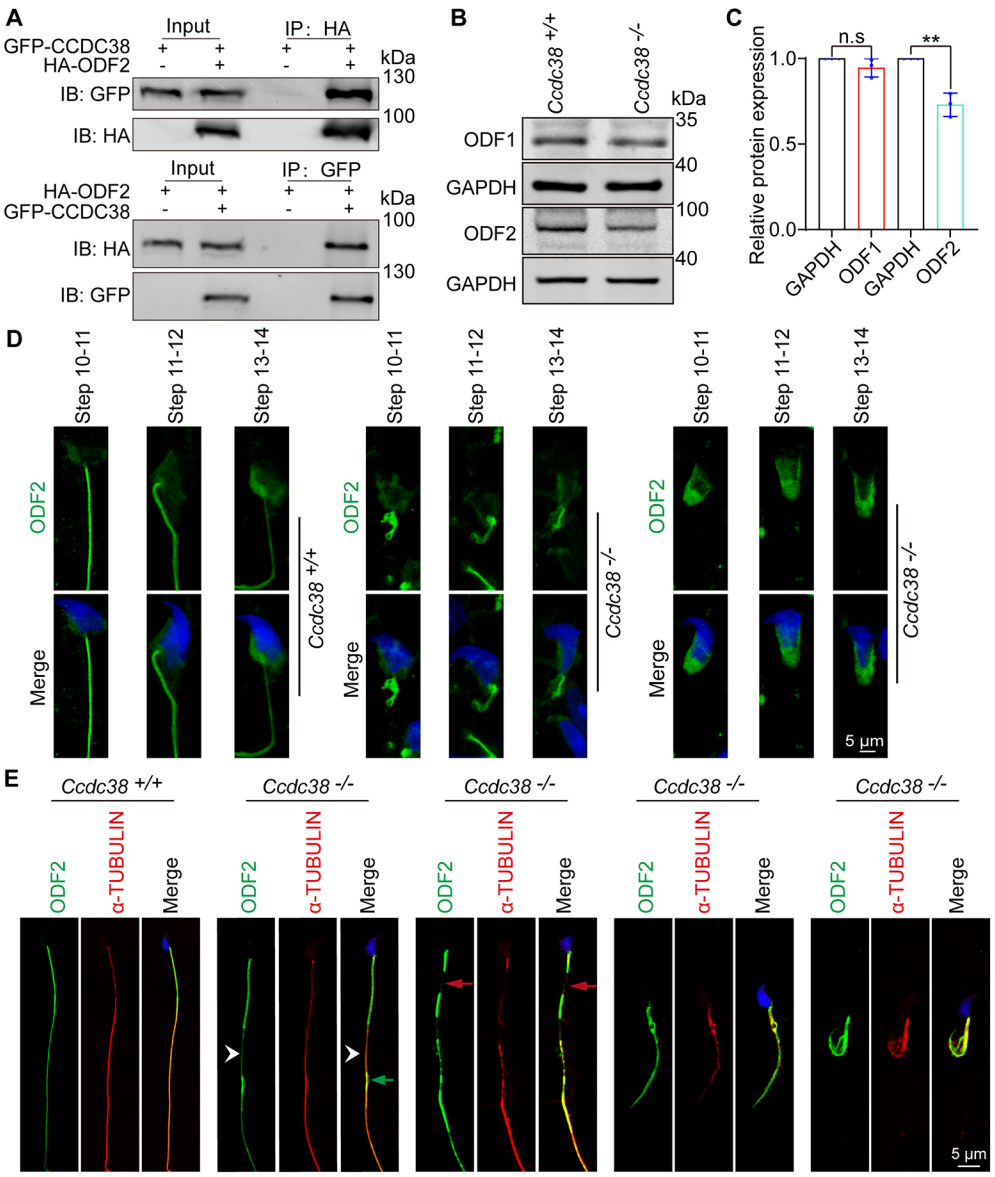

Fig. 8. ODF2 transportation is impaired in *Ccdc38*-knockout spermatids. (A) CCDC38 interacted with ODF2. pCDNA-HA-ODF2 and pEGFP-C1-CCDC38 plasmids were transfected into HEK293T cells. 48 h after transfection, cell lysates were collected for immunoprecipitation with the anti-GFP or anti-HA antibodies, and then analyzed using the anti-GFP or anti-HA antibodies. IB, immunoblotting; IP, immunoprecipitation. (B) Western blots showing ODF1 and ODF2 protein levels in lysates from *Ccdc38*$^{+/+}$ and *Ccdc38*$^{-/-}$ mice testes. GAPDH served as a loading control. ODF2 protein levels were reduced in *Ccdc38*$^{-/-}$ testes compared with *Ccdc38*$^{+/+}$ testes. (C) Quantitative results of the western blot. Data are presented as the mean±s.d. n.s., not significant; $^{**}P<0.01$ (paired two-tailed Student's *t*-test). (D) The localization of ODF2 in testis germ cells. Testicular germ cells were stained using the anti-ODF2 antibody (green). ODF2 localized on the manchette and sperm tail in *Ccdc38*$^{+/+}$ spermatids (left panel). ODF2 localized on the manchette and sperm tail in some *Ccdc38*$^{-/-}$ spermatids (the middle panel), but only localized on the manchette in the other *Ccdc38*$^{-/-}$ spermatids (right panel). (E) Immunofluorescence of ODF2 (green) and α-tubulin (red) in spermatozoa released from the caudal epididymis of *Ccdc38*$^{+/+}$ and *Ccdc38*$^{-/-}$ mice. Nuclei were stained with DAPI (blue). Green arrow indicates disordered axoneme, white arrowheads indicate tenuous axoneme (the second panel) and red arrows indicate discontinuous, punctiform short axoneme (the third panel). Images are representative of five experiments. Scale bars: 5 μm.

One Step Cloning Kit (C115, Vazyme). Mouse *Ccdc38* was obtained from mouse testis cDNA and it was cloned into the pEGFP-C1 vector. Mouse I*ft20* was obtained from mouse testis cDNA and it was cloned into the pRK vector. Mouse *Odf2* was obtained from mouse testis cDNA and it was cloned into the pCDNA-HA-3.0 vector. pcDNA-HA-3.1 vector was obtained from Addgene (128034). pCSII-Myc and pEGFP-C1 vectors were obtained from BioVector NTCC. pRK-flag vector was modified from pRK7-N-Flag (BioVector NTCC).

Animals

The mouse *Ccdc38* gene is 1692 bp and contains 16 exons. *Ccdc38*-knockout mice were generated using the CRISPR/Cas9 system from Cyagen Biosciences. The genotyping primers used for knockout were: F1, 5′-GTAGCTGTTTCTAAGCGATCATCA-3′; R1, 5′-ACTAGGTACCTCAAGCTGGTTTAGA-3′. The genotyping primers for WT mice were: F1, 5′-GTAGCTGTTTCTAAGCGATCATCA-3′; R2, 5′-GTCATGGGACAGATGTGGAACTA-3′.

All animal experiments were performed according to approved institutional animal care and use committee (IACUC) protocols (#08-133) of the Institute of Zoology, Chinese Academy of Sciences, Beijing, China. All surgery was performed under sodium pentobarbital anesthesia, and every effort was made to minimize suffering.

Antibodies

The following primary antibodies were used for immunofluorescence (IF) and western blotting (WB): mouse anti-GFP (M20004, Abmart; 1:1000 for WB), rabbit anti-MYC (BE2011, EASYBIO; 1:1000 for WB), anti-ODF2 (12058-1-AP, Proteintech; 1:1000 for WB, 1:200 for IF), mouse anti-α-tubulin antibody (AC012, ABclonal, 1:100 for IF), mouse anti-α/β-tubulin antibody (ab44928, Abcam; 1:100 for IF), mouse anti-GAPDH antibody (AC002, ABclonal; 1:10,000 for WB), mouse anti-ODF1 antibody (sc-390152, Santa Cruz Biotechnology; 1:500 for WB), mouse anti-Ac-tubulin antibody (T7451, Sigma-Aldrich; 1:200 for IF), mouse anti-CCDC38 (generated by Dia-an Biotechnology, Wuhan, China; 1:20 for IF) and rabbit anti-CCDC38 (generated by Dia-an Biotechnology, Wuhan, China; 1:500 for WB). The Alexa Fluor 488 conjugate of lectin PNA (1:400, L21409, Thermo Fisher Scientific) was used for immunofluorescence. The following secondary antibodies were used: goat anti-rabbit FITC (1:200, ZF-0311, http://www.zsbio.com/), goat anti-TRITC (1:200, ZF-0316, Zhong Shan Jin Qiao), goat anti-mouse FITC (1:200, ZF-0312, Zhong Shan Jin Qiao) and goat anti-rabbit TRITC (1:200, ZF0313, Zhong Shan Jin Qiao).

Western blotting

As previously reported (Liu et al., 2016), the tunica albuginea of the testis was peeled and added to RIPA buffer supplemented with 1 mM

Development (2022) 149, dev200516. doi:10.1242/dev.200516

phenylmethylsulfonyl fluoride (PMSF) and protease inhibitor cocktail (PIC; Roche Diagnostics, 04693132001). The solution was sonicated transiently and then placed on ice for 30 min. The samples were centrifuged at 13,523 ***g*** for 15 min at 4°C. Next, the supernatants were collected in new tubes. Protein lysates were electrophoresed and electrotransferred to a nitrocellulose membrane. The membrane was then incubated with a primary antibody followed by a secondary antibody. Finally, the membrane was scanned using an Odyssey infrared imager (LI-COR Biosciences; RRID: SCR_014579).

Immunoprecipitation

Transfected cells were lysed in a lysis buffer (50 mM HEPES, pH 7.4, 250 mM NaCl, 0.1% NP-40 containing PIC and PMSF) on ice for 30 min and centrifuged at 13,523 ***g*** at 4°C for 15 min. Cell lysates were first incubated with a primary antibody (mouse anti-GFP antibody, M20004L; Abmart) overnight at 4°C and then incubated with protein A-Sepharose (GE, 17-1279-03) for 2 h at 4°C. The immunoprecipitates were washed three times with lysis buffer, the SDS loading buffer (2% SDS with 1 M DTT) added, heated for 10 min at 95°C and subjected to western blotting analysis.

Epididymal sperm count

The cauda epididymis was isolated from 8-week-old mice. Sperm was released from the cauda epididymis in human tubal fluid (HTF) medium (MR-070-D, Sigma-Aldrich) and incubated at 37°C for 15 min. The medium was then diluted to 1:100 and sperm were counted using a hemocytometer.

Tissue collection and histological analysis

As previously reported (Wang et al., 2018), the testes were dissected after euthanasia, and fixed with Bouin's fixative for 24 h at 4°C. Next, the testes were dehydrated with graded ethanol, embedded in paraffin and 5 µm sections were cut and placed on glass slides. Sections were stained with H&E and PAS for histological analysis after deparaffinization.

Transmission electron microscopy

Testes were processed using methods previously reported, with some modifications (Liu et al., 2016). Briefly, the testis from WT and *Ccdc38*-knockout mice testes and epididymides were dissected and fixed in 2.5% (v/v) glutaraldehyde in 0.1 M cacodylate buffer (6131-99-3, Sigma-Aldrich) at 4°C overnight. After washing in 0.1 M cacodylate buffer, samples were cut into small pieces, then immersed in 1% OsO_4 for 1 h at 4°C. Samples were dehydrated through a graded acetone series (50%, 60%, 70%, 80%, 90%, 95%, 100%) and embedded in resin [DDSA, NMA, enhancer, 812 (Sigma-Aldrich)] for staining. Ultrathin sections of 60 nm were cut and stained with uranyl acetate and lead citrate. Images were acquired and analyzed using a JEM-1400 transmission electron microscope (JEM-1400, JEOL).

Scanning electron microscopy

Sperm was released from the epididymis in HTF medium at 37°C for 15 min, centrifuged for 5 min at 500 ***g***, washed twice with a phosphate buffer (NaH_2PO_4 and $Na_2HPO_4{\cdot}12H_2O$) and fixed in 2.5% glutaraldehyde solution overnight. Samples were finally dehydrated in graded ethanol, subjected to drying and coated with gold. Images were acquired and analyzed using a SU8010 scanning electron microscope (SU8010, JEOL).

Immunofluorescence

The tunica albuginea of the testis was peeled and incubated with collagenase IV (17104019, Gibco) and hyaluronidase (H1115000, Sigma-Aldrich) in PBS for 15 min at 37°C, then washed twice with PBS. Next, the sample was fixed with 4% paraformaldehyde for 5 min, and then coated on a glass slide to dry. The slides were washed with PBS three times, treated with 0.5% Triton X-100 for 5 min, and finally blocked with 5% bovine serum albumin for 30 min. The samples were incubated with primary antibodies at 4°C overnight, followed by incubation with secondary antibodies for 1 h at room temperature and DAPI staining. Images were taken using LSM880 (Zeiss) and Sp8 (Leica) microscopes.

Reverse transcription-quantitative PCR (RT-qPCR)

Total RNA was extracted from mice tissues using TRIzol (Invitrogen; Thermo Fisher Scientific). The cDNA was synthesized using PrimeScript RT Regent Kit (Takara, RR037A). The primer sequences were: *Gapdh* F,5'-AGTGGCAAAGTGGAGATT-3′; *Gapdh* R, 5′-GTGGAGTCATACTG-GAACA-3′; *Ccdc38* F, 5′-CTTGTCCTGTTAGTCCTGTATAG-3′; *Ccdc38* R, 5′-CGTAGAGATGAAGTGTGATGAT-3′.

Statistical analysis

All data are presented as the mean±s.d. Statistical significance of the differences between the mean values for the various genotypes was measured by Student's *t*-tests with paired, two-tailed distribution. The data were considered significant for $*P<0.05$, $**P<0.01$ or $***P<0.001$.

Acknowledgements

We thank the State Key Laboratory of Membrane Biology, Institute of Zoology, Chinese Academy of Sciences for our electron microscopy work. We are grateful to Pengyan Xia for his help in preparing the electron microscopy samples and we thank Jingnan Liang (Institute of Microbiology, Chinese Academy of Sciences) for TEM technical support.

Competing interests

The authors declare no competing or financial interests.

Author contributions

Conceptualization: W.L., L.Y.; Methodology: X.W., L.W., S.X., Y.C., H.W., Z.Z., H.J.; Resources: F.G.; Data curation: R.Z.; Writing - review & editing: R.Z., B.W.; Project administration: C.L.

Funding

This work was funded by the National Science Fund for Distinguished Young Scholars (81925015), the National Natural Science Foundation of China (91649202) and the Strategic Priority Research Program of the Chinese Academy of Sciences (grant XDA16020701).

Peer review history

The peer review history is available online at https://journals.biologists.com/dev/article-lookup/doi/10.1242/dev.200516.

References

Azizi, F. and Ghafouri-Fard, S. (2017). Outer dense fiber proteins: bridging between male infertility and cancer. *Arch. Iran. Med.* **20**, 320-325.

Coutton, C., Escoffier, J., Martinez, G., Arnoult, C. and Ray, P. F. (2015). Teratozoospermia: spotlight on the main genetic actors in the human. *Hum. Reprod. Update* **21**, 455-485. doi:10.1093/humupd/dmv020

Donkor, F. F., Mönnich, M., Czirr, E., Hollemann, T. and Hoyer-Fender, S. (2004). Outer dense fibre protein 2 (ODF2) is a self-interacting centrosomal protein with affinity for microtubules. *J. Cell Sci.* **117**, 4643-4651. doi:10.1242/jcs.01303

Fawcett, D. W. (1975). The mammalian spermatozoon. *Dev. Biol.* **44**, 394-436. doi:10.1016/0012-1606(75)90411-X

Firat-Karalar, E. N., Sante, J., Elliott, S. and Stearns, T. (2014). Proteomic analysis of mammalian sperm cells identifies new components of the centrosome. *J. Cell Sci.* **127**, 4128-4133. doi:10.1242/jcs.157008

Freitas, M. J., Vijayaraghavan, S. and Fardilha, M. (2017). Signaling mechanisms in mammalian sperm motility. *Biol. Reprod.* **96**, 2-12. doi:10.1095/biolreprod.116.144337

Funabashi, T., Katoh, Y., Okazaki, M., Sugawa, M. and Nakayama, K. (2018). Interaction of heterotrimeric kinesin-II with IFT-B-connecting tetramer is crucial for ciliogenesis. *J. Cell Biol.* **217**, 2867-2876. doi:10.1083/jcb.201801039

Griswold, M. D. (2016). Spermatogenesis: the commitment to meiosis. *Physiol. Rev.* **96**, 1-17. doi:10.1152/physrev.00013.2015

Inaba, K. (2011). Sperm flagella: comparative and phylogenetic perspectives of protein components. *Mol. Hum. Reprod.* **17**, 524-538. doi:10.1093/molehr/gar034

Ishikawa, H. and Marshall, W. F. (2017). Intraflagellar transport and ciliary dynamics. *Cold Spring Harb. Perspect. Biol.* **9**, a021998. doi:10.1101/cshperspect.a021998

Ito, C., Akutsu, H., Yao, R., Yoshida, K., Yamatoya, K., Mutoh, T., Makino, T., Aoyama, K., Ishikawa, H., Kunimoto, K. et al. (2019). Odf2 haploinsufficiency causes a new type of decapitated and decaudated spermatozoa, Odf2-Dds, in mice. *Sci. Rep.* **9**, 14249. doi:10.1038/s41598-019-50516-2

Jiao, S.-Y., Yang, Y.-H. and Chen, S.-R. (2021). Molecular genetics of infertility: loss-of-function mutations in humans and corresponding knockout/mutated mice. *Hum. Reprod. Update* **27**, 154-189. doi:10.1093/humupd/dmaa034

Kierszenbaum, A. L. (2002). Intramanchette transport (IMT): managing the making of the spermatid head, centrosome, and tail. *Mol. Reprod. Dev.* **63**, 1-4. doi:10.1002/mrd.10179

Kierszenbaum, A. L., Gil, M., Rivkin, E. and Tres, L. L. (2002). Ran, a GTP-binding protein involved in nucleocytoplasmic transport and microtubule nucleation, relocates from the manchette to the centrosome region during rat spermiogenesis. *Mol. Reprod. Dev.* **63**, 131-140. doi:10.1002/mrd.10164

Kim, Y. H., Mcfarlane, J. R., O'bryan, M. K., Almahbobi, G., Temple-Smith, P. D. and de Kretser, D. M. (1999). Isolation and characterization of rat sperm tail outer dense fibres and comparison with rabbit and human spermatozoa using a polyclonal antiserum. *J. Reprod. Fertil.* **116**, 345-353. doi:10.1530/jrf.0.1160345

Lehti, M. S. and Sironen, A. (2016). Formation and function of the manchette and flagellum during spermatogenesis. *Reproduction* **151**, R43-R54. doi:10.1530/REP-15-0310

Lehti, M. S. and Sironen, A. (2017). Formation and function of sperm tail structures in association with sperm motility defects. *Biol. Reprod.* **97**, 522-536. doi:10.1093/biolre/iox096

Li, Y., Sha, Y., Wang, X., Ding, L., Liu, W., Ji, Z., Mei, L., Huang, X., Lin, S., Kong, S. et al. (2019). DNAH2 is a novel candidate gene associated with multiple morphological abnormalities of the sperm flagella. *Clin. Genet.* **95**, 590-600. doi:10.1111/cge.13525

Li, L., Feng, F., Wang, Y., Guo, J. and Yue, W. (2020). Mutational effect of human CFAP43 splice-site variant causing multiple morphological abnormalities of the sperm flagella. *Andrologia* **52**, e13575. doi:10.1111/and.13575

Lin, S.-R., Li, Y.-C., Luo, M.-L., Guo, H., Wang, T.-T., Chen, J.-B., Ma, Q., Gu, Y.-L., Jiang, Z.-M. and Gui, Y.-T. (2016). Identification and characteristics of the testes-specific gene, Ccdc38, in mice. *Mol. Med. Rep.* **14**, 1290-1296. doi:10.3892/mmr.2016.5360

Liu, C., Wang, H., Shang, Y., Liu, W., Song, Z., Zhao, H., Wang, L., Jia, P., Gao, F., Xu, Z. et al. (2016). Autophagy is required for ectoplasmic specialization assembly in sertoli cells. *Autophagy* **12**, 814-832. doi:10.1080/15548627.2016.1159377

Liu, W., He, X., Yang, S., Zouari, R., Wang, J., Wu, H., Kherraf, Z.-E., Liu, C., Coutton, C., Zhao, R. et al. (2019). Bi-allelic mutations in TTC21A induce asthenoteratospermia in humans and mice. *Am. J. Hum. Genet.* **104**, 738-748. doi:10.1016/j.ajhg.2019.02.020

Liu, C., Miyata, H., Gao, Y., Sha, Y., Tang, S., Xu, Z., Whitfield, M., Patrat, C., Wu, H., Dulioust, E. et al. (2020). Bi-allelic DNAH8 variants lead to multiple morphological abnormalities of the sperm flagella and primary male infertility. *Am. J. Hum. Genet.* **107**, 330-341. doi:10.1016/j.ajhg.2020.06.004

Pasek, R. C., Malarkey, E., Berbari, N. F., Sharma, N., Kesterson, R. A., Tres, L. L., Kierszenbaum, A. L. and Yoder, B. K. (2016). Coiled-coil domain containing 42 (Ccdc42) is necessary for proper sperm development and male fertility in the mouse. *Dev. Biol.* **412**, 208-218. doi:10.1016/j.ydbio.2016.01.042

Pereira, R., Sa, R., Barros, A. and Sousa, M. (2017). Major regulatory mechanisms involved in sperm motility. *Asian J. Androl.* **19**, 5-14. doi:10.4103/1008-682X.167716

Perles, Z., Cinnamon, Y., Ta-Shma, A., Shaag, A., Einbinder, T., Rein, A. J. J. T. and Elpeleg, O. (2012). A human laterality disorder associated with recessive CCDC11 mutation. *J. Med. Genet.* **49**, 386-390. doi:10.1136/jmedgenet-2011-100457

Priyanka, P. P. and Yenugu, S. (2021). Coiled-coil domain-containing (CCDC) proteins: functional roles in general and male reproductive physiology. *Reprod. Sci.* **28**, 2725-2734. doi:10.1007/s43032-021-00595-2

Qian, X., Wang, L., Zheng, B., Shi, Z.-M., Ge, X., Jiang, C.-F., Qian, Y.-C., Li, D.-M., Li, W., Liu, X. et al. (2016). Deficiency of Mkrn2 causes abnormal spermiogenesis and spermiation, and impairs male fertility. *Sci. Rep.* **6**, 39318. doi:10.1038/srep39318

Rosenbaum, J. L. and Witman, G. B. (2002). Intraflagellar transport. *Nat. Rev. Mol. Cell Biol.* **3**, 813-825. doi:10.1038/nrm952

San Agustin, J. T., Pazour, G. J. and Witman, G. B. (2015). Intraflagellar transport is essential for mammalian spermiogenesis but is absent in mature sperm. *Mol. Biol. Cell* **26**, 4358-4372. doi:10.1091/mbc.E15-08-0578

Scholey, J. M. (2003). Intraflagellar transport. *Annu. Rev. Cell Dev. Biol.* **19**, 423-443. doi:10.1146/annurev.cellbio.19.111401.091318

Sha, Y.-W., Ding, L. and Li, P. (2014). Management of primary ciliary dyskinesia/Kartagener's syndrome in infertile male patients and current progress in defining the underlying genetic mechanism. *Asian J. Androl.* **16**, 101-106. doi:10.4103/1008-682X.122192

Sha, Y.-W., Xu, X., Mei, L.-B., Li, P., Su, Z.-Y., He, X.-Q. and Li, L. (2017). A homozygous CEP135 mutation is associated with multiple morphological abnormalities of the sperm flagella (MMAF). *Gene* **633**, 48-53. doi:10.1016/j.gene.2017.08.033

Sha, Y., Xu, Y., Wei, X., Liu, W., Mei, L., Lin, S., Ji, Z., Wang, X., Su, Z., Qiu, P. et al. (2019). CCDC9 is identified as a novel candidate gene of severe asthenozoospermia. *Syst. Biol. Reprod. Med.* **65**, 465-473. doi:10.1080/19396368.2019.1655812

Shen, Y., Zhang, F., Li, F., Jiang, X., Yang, Y., Li, X., Li, W., Wang, X., Cheng, J., Liu, M. et al. (2019). Loss-of-function mutations in QRICH2 cause male infertility with multiple morphological abnormalities of the sperm flagella. *Nat. Commun.* **10**, 433. doi:10.1038/s41467-018-08182-x

Silva, E., Betleja, E., John, E., Spear, P., Moresco, J. J., Zhang, S., Yates, J. R., III, Mitchell, B. J. and Mahjoub, M. R. (2016). Ccdc11 is a novel centriolar satellite protein essential for ciliogenesis and establishment of left-right asymmetry. *Mol. Biol. Cell* **27**, 48-63. doi:10.1091/mbc.E15-07-0474

Sironen, A., Shoemark, A., Patel, M., Loebinger, M. R. and Mitchison, H. M. (2020). Sperm defects in primary ciliary dyskinesia and related causes of male infertility. *Cell. Mol. Life Sci.* **77**, 2029-2048. doi:10.1007/s00018-019-03389-7

Tang, S., Wang, X., Li, W., Yang, X., Li, Z., Liu, W., Li, C., Zhu, Z., Wang, L., Wang, J. et al. (2017). Biallelic mutations in CFAP43 and CFAP44 cause male infertility with multiple morphological abnormalities of the sperm flagella. *Am. J. Hum. Genet.* **100**, 854-864. doi:10.1016/j.ajhg.2017.04.012

Tapia Contreras, C. and Hoyer-Fender, S. (2019). CCDC42 localizes to Manchette, HTCA and tail and interacts with ODF1 and ODF2 in the formation of the male germ cell cytoskeleton. *Front. Cell Dev. Biol.* **7**, 151. doi:10.3389/fcell.2019.00151

Tarnasky, H., Cheng, M., Ou, Y., Thundathil, J. C., Oko, R. and van der Hoorn, F. A. (2010). Gene trap mutation of murine outer dense fiber protein-2 gene can result in sperm tail abnormalities in mice with high percentage chimaerism. *BMC Dev. Biol.* **10**, 67. doi:10.1186/1471-213X-10-67

Taschner, M. and Lorentzen, E. (2016). The intraflagellar transport machinery. *Cold Spring Harb. Perspect. Biol.* **8**, a028092. doi:10.1101/cshperspect.a028092

Wang, L., Tu, Z., Liu, C., Liu, H., Kaldis, P., Chen, Z. and Li, W. (2018). Dual roles of TRF1 in tethering telomeres to the nuclear envelope and protecting them from fusion during meiosis. *Cell Death Differ.* **25**, 1174-1188. doi:10.1038/s41418-017-0037-8

Wei, Y.-L. and Yang, W.-X. (2018). The acroframosome-acroplaxome-manchette axis may function in sperm head shaping and male fertility. *Gene* **660**, 28-40. doi:10.1016/j.gene.2018.03.059

Wu, B., Yu, X., Liu, C., Wang, L., Huang, T., Lu, G., Chen, Z.-J., Li, W. and Liu, H. (2021). Essential role of CFAP53 in sperm flagellum biogenesis. *Front. Cell Dev. Biol.* **9**, 676910. doi:10.3389/fcell.2021.676910

Yamaguchi, A., Kaneko, T., Inai, T. and Iida, H. (2014). Molecular cloning and subcellular localization of Tektin2-binding protein 1 (Ccdc 172) in rat spermatozoa. *J. Histochem. Cytochem.* **62**, 286-297. doi:10.1369/0022155413520607

Yang, K., Meinhardt, A., Zhang, B., Grzmil, P., Adham, I. M. and Hoyer-Fender, S. (2012). The small heat shock protein ODF1/HSPB10 is essential for tight linkage of sperm head to tail and male fertility in mice. *Mol. Cell. Biol.* **32**, 216-225. doi:10.1128/MCB.06158-11

Yang, K., Grzmil, P., Meinhardt, A. and Hoyer-Fender, S. (2014). Haplo-deficiency of ODF1/HSPB10 in mouse sperm causes relaxation of head-to-tail linkage. *Reproduction* **148**, 499-506. doi:10.1530/REP-14-0370

Young, S. A., Miyata, H., Satouh, Y., Kato, H., Nozawa, K., Isotani, A., Aitken, R. J., Baker, M. A. and Ikawa, M. (2015). CRISPR/Cas9-mediated rapid generation of multiple mouse lines identified Ccdc63 as essential for spermiogenesis. *Int. J. Mol. Sci.* **16**, 24732-24750. doi:10.3390/ijms161024732

Zhu, Z.-J., Wang, Y.-Z., Wang, X.-B., Yao, C.-C., Zhao, L.-Y., Zhang, Z.-B., Wu, Y., Chen, W. and Li, Z. (2022). Novel mutation in ODF2 causes multiple morphological abnormalities of the sperm flagella in an infertile male. *Asian J. Androl.* **24**, 1-10. doi:10.4103/aja202183

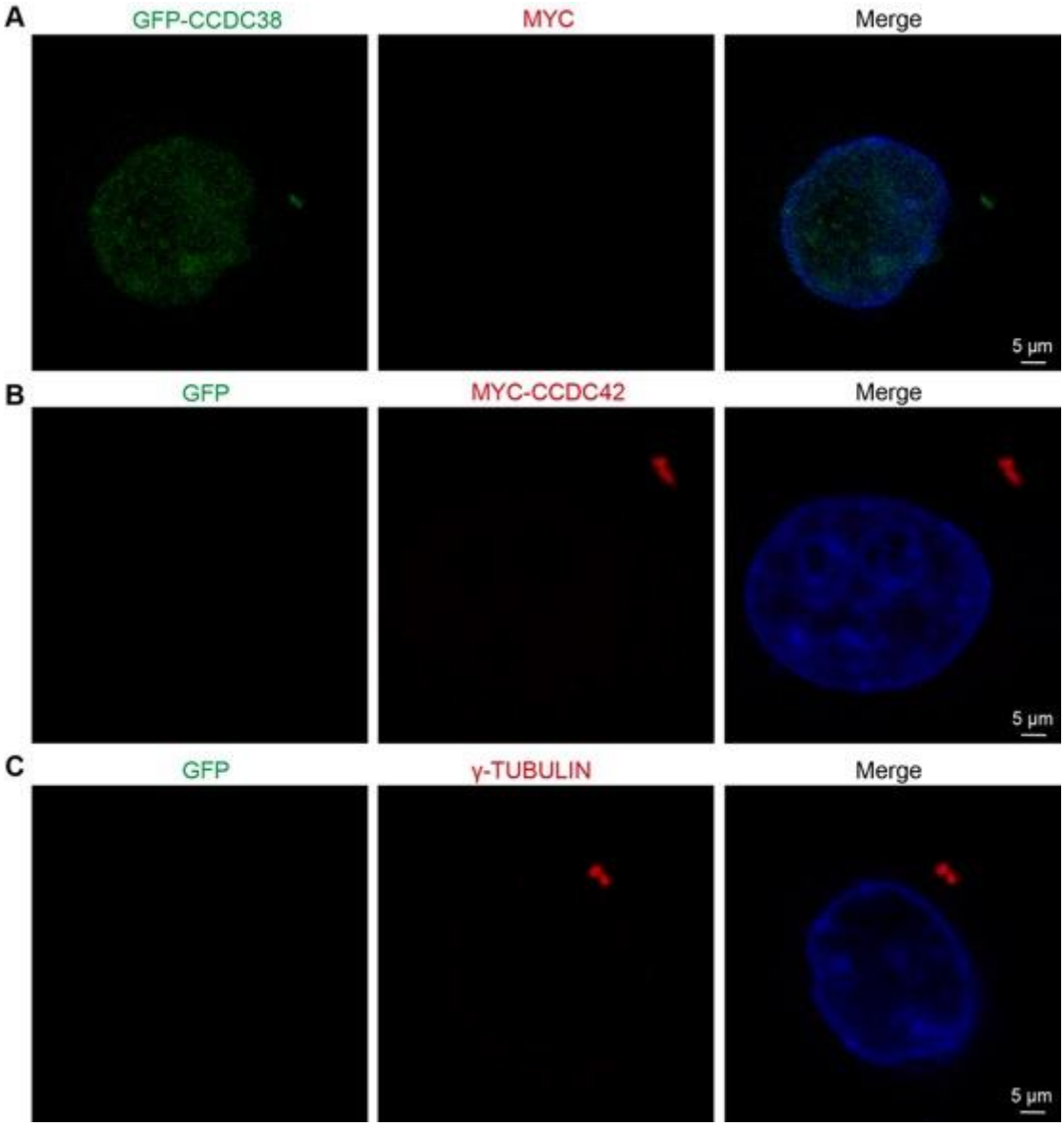

Fig. S1. Immunofluorescence analysis shows the localization of CCDC38 in somatic cells. (A-B) Immunofluorescence analysis using anti-GFP (green) and anti-MYC (red) antibodies was performed in Hela cells. Nuclei were stained with DAPI (blue). (C) Immunofluorescence analysis using anti-GFP (green) and anti-γ-TUBULIN (red) antibodies were performed in Hela cells. Nuclei were stained with DAPI (blue). Scale bars: 5 μm.

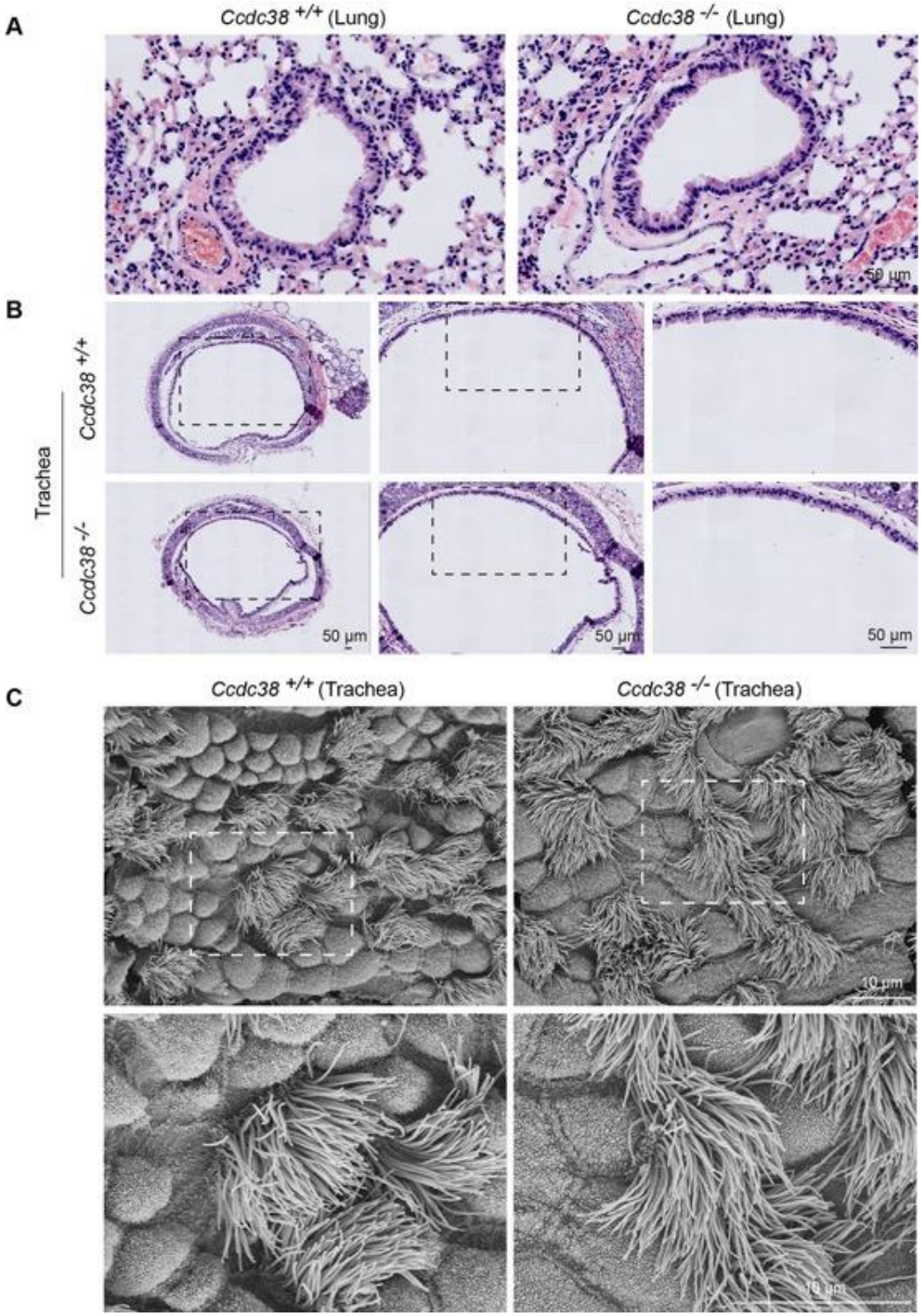

Fig. S2. Trachea cilia and lung cilia appear normal in *Ccdc38*$^{-/-}$ mice. (A) The histology of the lung from *Ccdc38*$^{+/+}$ and *Ccdc38*$^{-/-}$ mice. (B) The histology of the trachea from *Ccdc38*$^{+/+}$ and *Ccdc38*$^{-/-}$ mice. (C) Scanning electron micrography of *Ccdc38*$^{+/+}$ and *Ccdc38*$^{-/-}$ tracheal epithelium at low (upper) and high magnifications of the boxed areas (lower). Scale bars: 50 μm (A, B); 10 μm (C).

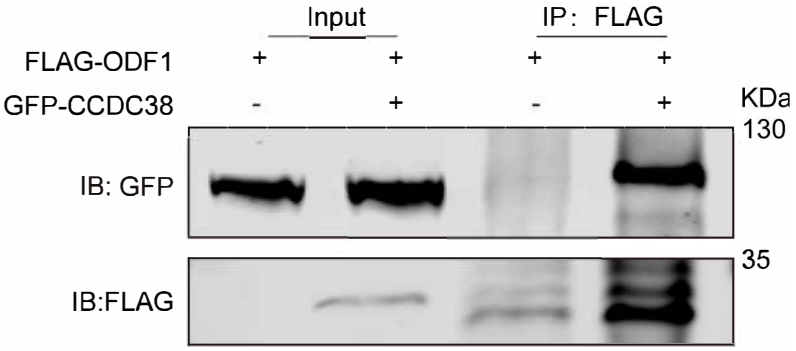

Fig. S3. CCDC38 can interact with ODF1. pRK-FLAG-ODF1 and pEGFP-C1-CCDC38 plasmids were transfected into HEK293T cells. Forty-eight hours after transfection, cells were collected for immunoprecipitation with anti-FLAG and analyzed with GFP or FLAG antibodies, respectively.